Electronic Supplementary Information (ESI) of the manuscript

Unlocking Superior NO_2 Sensitivity and Selectivity: The Role of Sulfur Abstraction in Indium Sulfide (InS) Nanosheets-Based Sensors

Gianluca D'Olimpio [1], Danil W. Boukhvalov [2,*], Vardan Galstyan [3], Jessica Occhiuzzi [1], Michael Vorochta [4], Matteo Amati [5], Zygmunt Milosz [5], Luca Gregoratti [5], Marian Cosmin Istrate [6], Chia-Nung Kuo [7], Chin Shan Lue [7], Corneliu Ghica [6], Elisabetta Comini [3,], Antonio Politano [1,*]

[1] *Department of Physical and Chemical Sciences, University of L'Aquila, via Vetoio, 67100 L'Aquila (AQ), Italy*
[2] *College of Science, Institute of Materials Physics and Chemistry, Nanjing Forestry University, Nanjing 210037, P. R. China*
[3] *Sensor Lab, Department of Information Engineering, University of Brescia, Via Valotti 9, 25133 Brescia, Italy*

[4] *Faculty of Mathematics and Physics, Charles University, V Holešovičkách 2, Prague 8, 18000 Prague, Czech Republic*

[5] *Elettra - Sincrotrone Trieste SCpA, AREA Science Park, Strada Statale 14 km 163.5, 34149, Trieste, Italy*

[6] *National Institute of Materials Physics, Atomistilor 405A, 077125 Magurele, Romania*

[7] *Department of Physics, National Cheng Kung University, 1 Ta-Hsueh Road, 70101 Tainan, Taiwan*

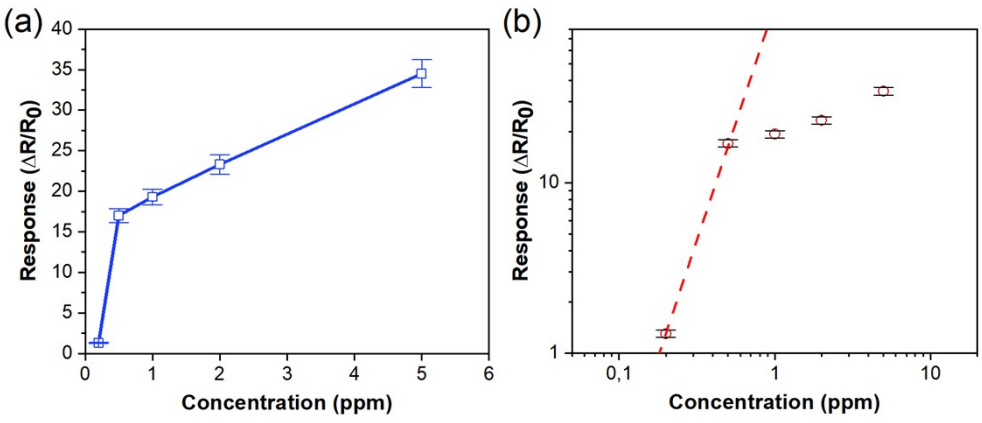

Figure S1. (a) Response vs. NO_2 concentration (0.2, 0.5, 1, 2, and 5 ppm) dependence of InS at optimum operating temperature (400 °C, RH, 40%). (b) Calibration curve of the normalized

sensing response of InS to NO_2 at 400 °C. We set the response value ($\Delta R/R_0$) of the InS sensor to 1 to estimate the LOD.

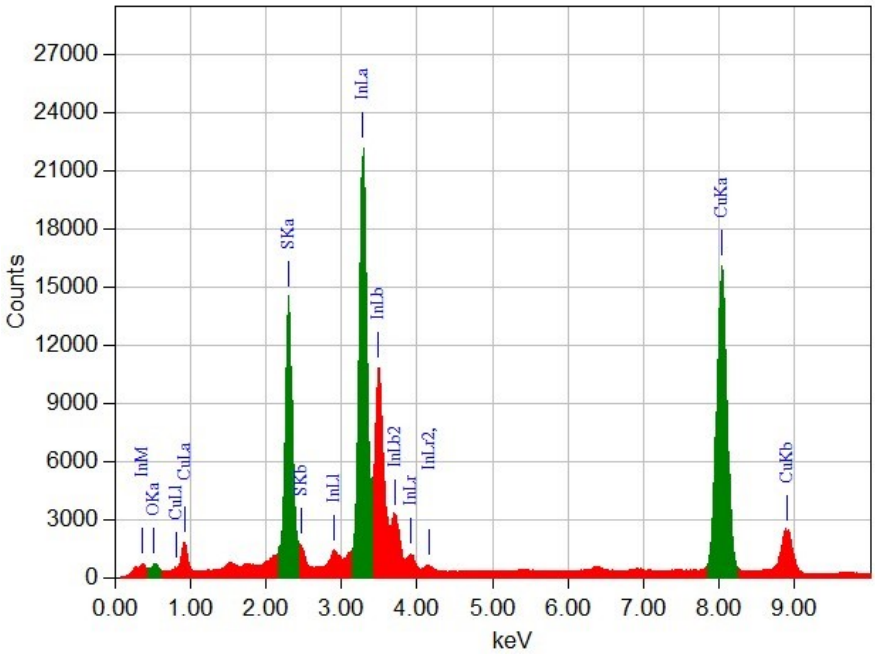

Figure S2: EDS spectrum indicating the presence of oxygen along with the main elements indium and sulfur.

The X-ray diffraction (XRD) studies clearly demonstrate the integrity of the crystal structure even in these extreme conditions, exhibiting no observable changes or phase transitions.

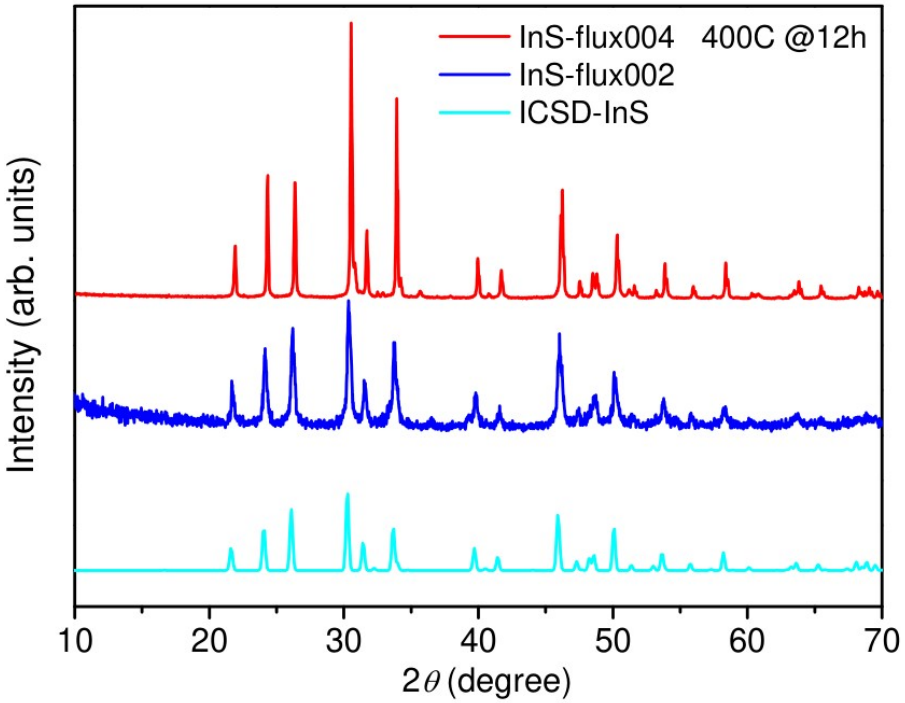

Figure S3: *XRD pattern of as-cleaved InS bulk single crystal at RT and 400°C.*

In addition, Figure S4 shows that Raman spectroscopy was used at room temperature, 200°C, and 400°C to confirm the stability of the crystal phase. The Raman spectra show changes in peak positions, primarily related to temperature-induced changes in phonon energy. These differences correspond to the effects of thermal disturbance and high temperatures on phonon behavior. Especially, the steady-state vibrational patterns at 400°C indicate that phase transitions are not present. Our results indicate that the Raman spectrum shifts that we have observed are mostly caused by changes in phonon behavior, which supports the material's stability over the temperature range that we have studied. The observed decrease in phonon energy with rising temperature is attributed to the intricate interplay between anharmonic effects and the thermal expansion of the crystal lattice. Anharmonicity induces phonon interaction, leading to energy redistribution within the lattice. Concurrently, the expansion of the crystal lattice at elevated temperatures results in a reduction in force constants governing atomic vibrations and a corresponding decrease in phonon frequency. This dynamic

relationship highlights the material's response to temperature. The changes in phonon population and energies, driven by anharmonic effects and the system's reaction to high temperatures, underscore the intricate nature of these vibrational dynamics, further accentuated by fluctuations in force constants due to thermal expansion.

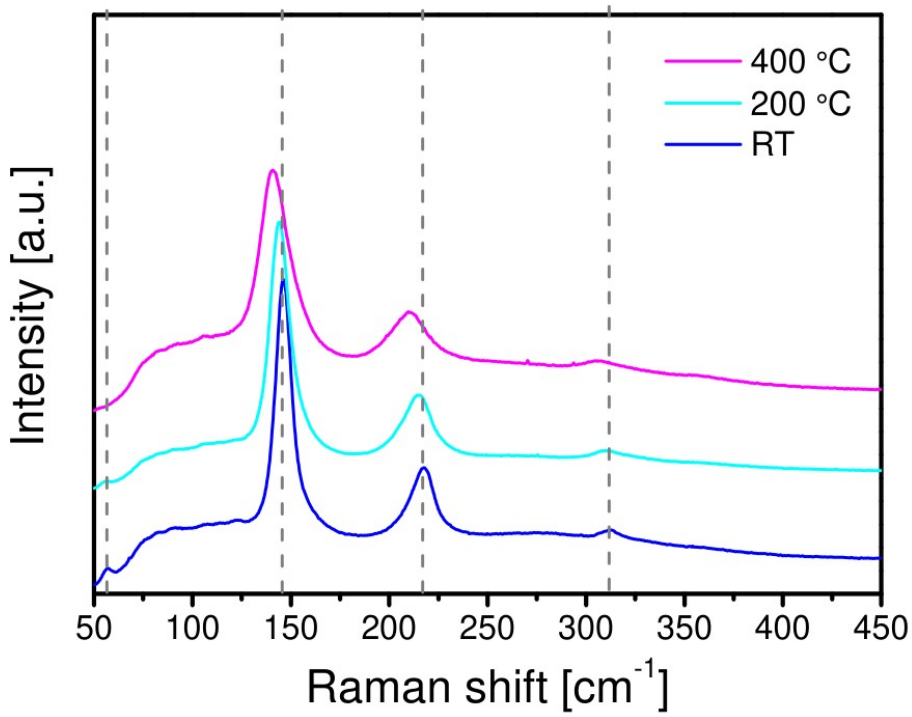

Figure S4: Raman spectra of InS at RT, 200°C and 400°C.

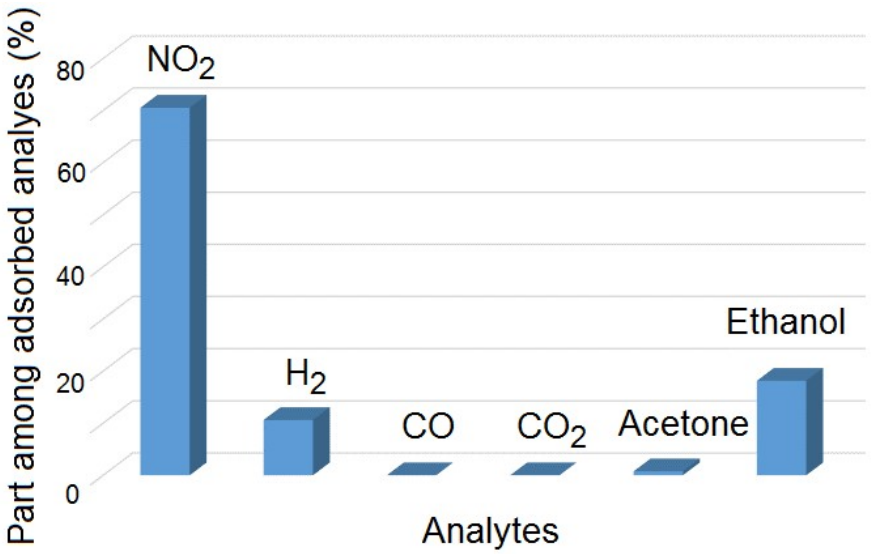

Figure S5. *Boltzmann distribution of analytes adsorbed on strained* $In_2O_{2.67}$ substrate at *400 °C.*

Table S1. *Comparison of gas sensing properties of InS with respect to state-of-the-art sensing structures based on 2D semiconductors and metal-oxide nanostructures.* V_a *denotes the output voltage of the sensor in air and* V_g *represents the output voltage under exposure to* NO_2.

Material	NO_2 concentration (ppm)	Response $[(R_f-R_0)/R_0]$	Operating temperature (°C)	Estimated LOD (ppb)
SnS_2 [1]	5	2.5	200	–
Sb_2Se_3 [2]	2	0.8, $(R_a-R_g)/R_a$	140	60
N-doped In_2S_3 [3]	10	0.1, $(R_a-R_g)/R_a$	RT	–
$SnO_2/SnSe_{1.7}$ [4]	1	2.2	150	360
In_2O_3/SnS_2 [5]	50	15,* V_g/V_a	25	–
In_2S_3/In_2O_3 [6]	1	24	160	
SnO_2/SnS_2 [7]	3	15.33, R_a/R_g	60	37
$SnSe_2$/SnO/SnSe [8]	5	2.6	RT	115
reduced graphene oxide [9]	1	0.6,§ $(G_f-G_0)/G_0$	450	50
Black phosphorus	25	0.2	RT	–
Al–Black phosphorus [10]	1	0.1	70	–
reduced graphene oxide/MoS_2 [11]	10	0.1	RT	–
C/g-C_3N_4 [12]	50	0.7	200	7390
In_2O_3 nanoparticles [13]	1.2	0.1, R_a/R_g	300	–

In_2O_3 nanoparticles [14]	40	6, R_a/R_g	225	–
In_2O_3 nanoparticles/SnO_2 nanowires [15]	5	24	300	–
SnO_2 nanowires [15]	5	2.3	300	–
InS (this work)	5	34.5	400	5

* Room temperature

§ G_0 is the baseline conductance value of the sensor in air and G_f is the steady-state conductance value of the sensor in the presence of NO_2.

References

1. M. Cheng, Z. Wu, G. Liu, L. Zhao, Y. Gao, B. Zhang, F. Liu, X. Yan, X. Liang, P. Sun and G. Lu, *Sens. Actuators B Chem.*, 2019, **291**, 216-225.
2. Y. B. Kim, S. H. Jung, D. S. Kim, N. G. Deshpande, H. W. Suh, H. H. Lee, J. H. Choi, H. S. Lee and H. K. Cho, *Adv. Funct. Mater.*, 2021, **31**, 2102439.
3. Y. Cheng, Z. Li, T. Tang, K. Xu, H. Yu, X. Tao, C. M. Hung, N. D. Hoa, Y. Fang, B. Ren, H. Chen and J. Z. Ou, *Applied Materials Today*, 2022, **26**, 101355.
4. V. Paolucci, G. D'Olimpio, C.-N. Kuo, C. S. Lue, D. W. Boukhvalov, C. Cantalini and A. Politano, 2020.
5. Y. Yang, D. Zhang, D. Wang, Z. Xu and J. Zhang, *J. Mater. Chem. A*, 2021, **9**, 14495-14506.
6. B.-R. Wang, L.-Y. Liu, G.-C. Guo, Y.-J. Bai, J.-C. Tu and R.-Z. Wang, *Appl. Surf. Sci.*, 2022, **584**, 152669.
7. H. Yang, C. Zhu, Q. Wu, X. Li, H. Wang, J. Wan, C. Xie and D. Zeng, *Appl. Surf. Sci.*, 2022, **601**, 154213.
8. S. Rani, M. Kumar, P. Garg, R. Parmar, A. Kumar, Y. Singh, V. Baloria, U. Deshpande and V. N. Singh, *ACS Appl. Mater. Interfaces*, 2022, **14**, 15381-15390.
9. S. Cui, H. Pu, E. C. Mattson, Z. Wen, J. Chang, Y. Hou, C. J. Hirschmugl and J. Chen, *Anal. Chem.*, 2014, **86**, 7516-7522.
10. G. Lee, S. Kim, S. Jung, S. Jang and J. Kim, *Sens. Actuators B Chem.*, 2017, **250**, 569-573.
11. B. Han, Z. Duan, J. Xu, Y. Zhu, Q. Xu, H. Wang, H. Tai, J. Weng and Y. Zhao, *Adv. Funct. Mater.*, 2020, **30**, 2002232.
12. A. Govind, P. Bharathi, G. Mathankumar, M. K. Mohan, J. Archana, S. Harish and M. Navaneethan, *Diamond Relat. Mater.*, 2022, **128**, 109205.
13. P. Sowti khiabani, E. Marzbanrad, H. Hassani and B. Raissi, *J. Am. Ceram. Soc.*, 2013, **96**, 2493-2498.
14. S. Shah, S. Han, S. Hussain, G. Liu, T. Shi, A. Shaheen, Z. Xu, M. Wang and G. Qiao, *Ceram. Int.*, 2022, **48**, 12291-12298.
15. S. Park, Y. W. Jung, G. M. Ko, D. Y. Jeong and C. Lee, *Applied Physics A*, 2021, **127**, 898.